Sigwadi et al. International Journal of Mechanical and Materials Engineering (2019) 14:5
https://doi.org/10.1186/s40712-019-0102-9

International Journal of Mechanical and Materials Engineering

ORIGINAL PAPER Open Access

Preparation of a high surface area zirconium oxide for fuel cell application

Rudzani Sigwadi[1*], Mokhotjwa Dhlamini[2], Touhami Mokrani[1] and Fulufhelo Nemavhola[3]

Abstract

Stable and high surface area zirconium oxide nanoparticles have been synthesised by means of the hydrothermal method. The Brunauer–Emmett–Teller results show that a high surface area of 543 m^2/g was obtained in the hydrothermal process, having a high porosity in nanometre range. The hydrothermal method was applied at 120 °C by using an autoclave with a Teflon liner at an ambient pressure for 48 h. High-resolution scanning electron microscopy shows the different morphologies of zirconia nanoparticles, which could be categorised as one-dimensional and zero-dimensional, as they had a high crystallite orientation, which was also confirmed by the X-ray diffraction (XRD). The mixture of two types of cubic phases in one sample was obtained from XRD and confirmed by the zirconia nanostructure, showing the stable phase of fluorite, which has full cubic symmetry (*Im*-3*m*), and also an Arkelite zirconia nanostructure, showing the stable phase of fluorite, which has full cubic symmetry (*Fm*-3*m*). The XRD results also show the different structure orientations of face-centred cubic and body-centred cubic in one sample.

Keywords: Face-centred cubic, Body-centred cubic, Autoclaves, Hydrothermal, Dimensional, Arkelite, Fluorite

Background

The synthesis of zirconium oxide nanoparticles (ZrO_2) in one-dimensional (1D) or three-dimensional (3D) form has attracted considerable research due to the excellent mechanical and chemical properties of these nanoparticles. 1D nanomaterials, such as nanoribbons, exhibit novel physical properties with potential application in a number of areas due to their high strength and fracture toughness, low thermal conductivity, high corrosion resistance, both acidic and basic properties and high melting point (Dong, Lin, Liu, & Li, 2009; Kalkur & Lu, 1992; Wang et al., 2009; Xu, Qin, Yang, & Li, 2003). Zirconia nanoparticles have been used in many applications such as solid oxide fuel cells, bio-sensors, H_2 gas storage materials, oxygen sensors, catalysts and catalyst support (Dwivedi, Maurya, Verma, Prasad, & Bartwal, 2011). Furthermore, zirconia, in the form of nanotubes or nanowires, is expected to improve the sensitivity of chemical sensors and reinforce thermal stability and toughness of the material (Hamling, 1997). Zirconia is known as a solid acid catalyst and an *n*-type semiconductor material (Reddy & Khan, 2005). It is also used as protection against chemical corrosion and metal oxidation (Ibáñez, Martin, Ramos-Barrado, & Leinen, 2006). ZrO_2 is highly conductive at elevated temperatures due to its wide band gap semiconductor properties (Kumari et al., 2009). Generally, zirconia nanoparticles consist of three crystalline structures, which are cubic (C), tetragonal (T) and monoclinic (M), depending on their transformation temperatures (cubic > 2370 °C, tetragonal > 1150 °C and monoclonic > 1150 °C) (Arantes et al., 2010). The change in volume associated with this transformation makes using pure zirconium oxide impossible in many applications (Singh & Nakate, 2014). Upon cooling, transformation is reversed spontaneously, the transformation is thermal and there is less diffusion. Furthermore, the tetragonal-to-monoclinic transformation occurs with a volume expansion of about 4–5%, inducing high compressive stresses in the material (Monaco, Tucci, Esposito, & Scotti, 2013). Zirconia with tetragonal and cubic structures has a higher density and a higher crystallisation temperature than the monoclinic structure (William, Callister, & David, 2012; Dercz, Prusik, & Pajak, 2008). The induced stress explanation depends upon the tetragonal-to-monoclinic transformation, once the application temperature surpasses the transformation temperature, at about 1000 °C. The high-temperature phases, such as

* Correspondence: sigwara@unisa.ac.za
[1]Department of Chemical Engineering, University of South Africa, Private Bag X6, Florida 1710, South Africa
Full list of author information is available at the end of the article

cubic and tetragonal, can be stabilised at room temperature by using stabilisers such as Y_2O_3, CaO, MgO and CeO_2 to avoid cracks within the structure due to the transformation phase (Lumpkin, 1999; Zhu, Shi, Liang, Hui, & Lau, 2008). The stabilised cubic ZrO_2 can also be used as an oxygen sensor in fuel cell membranes, because it has the ability to allow oxygen ions to move freely through the crystal structure at high temperatures (Ge et al., 2014; Kumari et al., 2009). The cubic phase possesses high oxygen ionic conductivity, low thermal conductivity and chemical stability over a wide range of temperatures and oxygen partial pressure (Behbahani, Rowshanzamir, & Esmaeilifar, 2012), which has led to its use as a thermal barrier coating in jet and diesel engines to allow operation at higher temperatures. Moreover, cubic zirconia conducts electricity very well when used in the form of small grain-sized units of less than 15 nm wide, which makes fuel cells much more reliable and less expensive. Since all fuel cells are based on oxides, this cubic zirconia nanomaterial would be beneficial, as it could replace or reduce the use of platinum, while reducing costs and increasing fuel cell efficiency. Its physical properties strongly depend on the phase and crystalline size (Babu, Reddy, & Reddy, 2015). In addition, researchers have introduced various synthesis methods such as microwave irradiation, hydrothermal, solid-state synthesis and sol gel, combined with solvent synthesis (Babu et al., 2015), to increase the crystal sizes and their morphological phases (Babu et al., 2015). The high-temperature phase of ZrO_2 could be used as reinforcement for toughening aluminium through phase transformation, phase conversion and microcracking (Xu et al., 2003). The successful synthesis of ZrO_2 nanotubes and nanofibres by direct electro-chemical anodisation and electrospinning has been reported (Kumari et al., 2009). Porous anodic aluminium oxide (AAO) templates are considered particularly attractive for fabricating nanotubes or nanowires (Kumari et al., 2009). It was reported that fabricating with an AAO template can produce ZrO_2 nanowire, which has high photoluminescence (Cao et al., 2004; Dong et al., 2009). The advantages of the hydrothermal method are that crystalline is produced at a lower temperature without using a great deal of energy (i.e. calcined at a high temperature), less agglomeration, good distribution of particle size and controlled morphology (Kumari et al., 2009). This paper reports on the hydrothermal method used to synthesise ZrO_2 nanostructure, such as nanorods and nanospheres, with pure cubic phases without any fabrication. Zirconia nanospheres and nanorods were obtained without using any alcohol, by applying the hydrothermal method at ambient pressure for 48 h, and using zirconium oxychloride hydrate and sodium hydroxide as precursor materials at 120 °C. Zirconium salt was used, as it is inexpensive and insensitive to the atmosphere.

Methods

Materials

Zirconium oxychloride hydrate ($ZrOCl_2{\cdot}8H_2O$), sodium hydroxide pellets (NaOH), ethanol, Nafion® solution, potassium chloride (KCl) and sodium nitrates ($NaNO_3$) were purchased from Sigma Aldrich. All the chemicals with analytical grade were used as received, without any further purification.

Preparation of zirconium oxide by hydrothermal method

The ZrO_2 nanoparticles were prepared by means of the hydrothermal method; $ZrOCl_2{\cdot}8H_2O$ and NaOH were used as starting materials (Sigwadi, Dhlamini, Mokrani, & Nonjola, 2017). Zirconium hydroxide's precipitation ($Zr(OH)_4$) was obtained by slowly adding 5 M NaOH to the aqueous solution of 0.5 M $ZrOCl_2{\cdot}8H_2O$, at room temperature, while continuously stirring with a magnetic stirrer and mixed for 30 min. The resulting solution was then transferred to an autoclave with a Teflon liner. The sample run was at a temperature of 120 °C, with 400 rps and zero bar pressure for 48 h. The resulting product was centrifuged and washed with distilled water until the pH was neutral. Then it was dried overnight at 80 °C.

Reaction:

$$ZrOCl_2 \cdot 8H_2O + NaOH = Zr(OH)_4 + NaCl_2 + H_2O \quad (1)$$

$$Zr(OH)_4 = ZrO_2 + 2H_2O \quad (2)$$

Characterisation

The X-ray diffraction (XRD) analysis was performed using a Philips automated X-ray diffractometer, with a CuK radiation source. Samples were scanned in continuous mode,

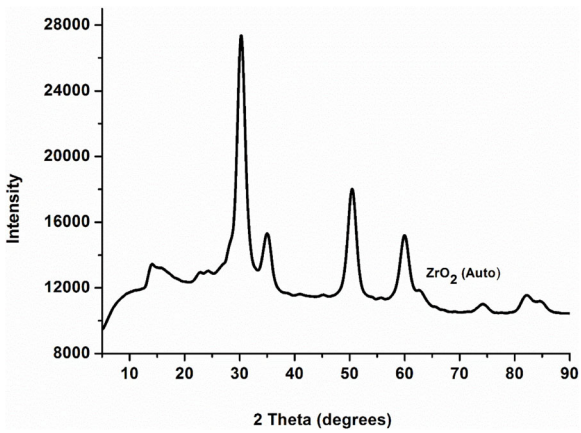

Fig. 1 The XRD patterns of the ZrO_2 nanoparticles

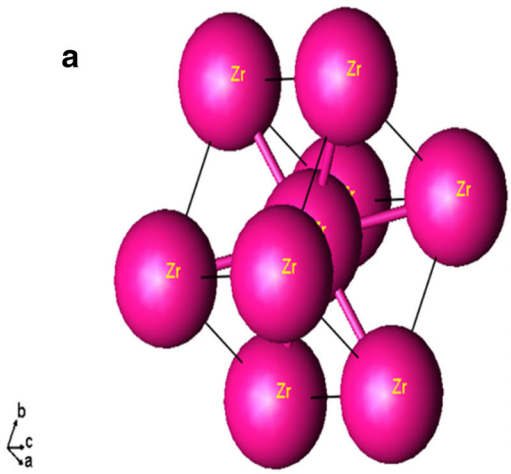

Data	Value
Chemical formula	Zr
Composition	Zr
Z-value	1.000
Concentration(%)	0.0292(11)
RIR value	19.233
DB card number	9008559
Crystal system	Cubic
Space group	229 : Im-3m
a(ang.)	3.6153
b(ang.)	3.6153
c(ang.)	3.6153
alpha(deg)	90.0000
beta(deg)	90.0000
gamma(deg)	90.0000
Calc. density(g/cm^3)	6.41150
Mass absorption coefficient(cm^2/g)	129.14480

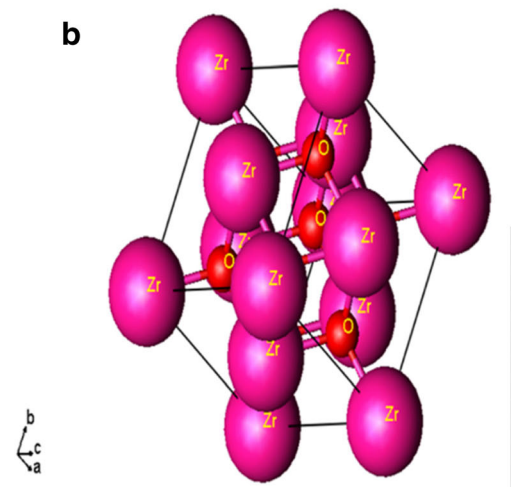

Data	Value
Chemical formula	O_2 Zr
Composition	O_2 Zr
Z-value	4.000
Concentration(%)	100(7)
RIR value	9.917
DB card number	5000038
Crystal system	Cubic
Space group	225 : Fm-3m
a(ang.)	5.1144
b(ang.)	5.1144
c(ang.)	5.1144
alpha(deg)	90.0000
beta(deg)	90.0000
gamma(deg)	90.0000
Calc. density(g/cm^3)	6.21360
Mass absorption coefficient(cm^2/g)	97.07250

Fig. 2 **a** Structure of zirconia nanostructure and **b** structure of Arkelite zirconia nanostructure with crystallographic information about Zr and Zr hydrides

from 5 to 90° (2θ), with a scanning rate of 0.026°/1 s). The thermal properties of the samples were studied using a thermal gravimetric analysis (TGA) under nitrogen flow. TGA data was obtained with a PerkinElmer instrument, over nitrogen and at a heating rate of 10 °C/min from 50 to 1000 °C. A Brunauer–Emmett–Teller (BET) surface area instrument (TriStar II 3020 Version 2) was used to determine information such as gas uptake, micropore volume (*t*-plot method) and pore size distribution via adsorption and desorption isotherms. In a BET surface area analysis, a dry sample was evacuated of all gas and cooled to 77 K, using liquid nitrogen. The morphology was investigated by means of a scanning electron microscope (SEM). SEM images were obtained on a Hitachi × 650. Electronic techniques were based on the interaction of the sample with electrons, which resulted in a secondary effect that was detected and measured. FT-IR spectroscopy was used to determine the quality and composition of the sample. FT-IR spectra were obtained with a (Perkin-Elmer Paragon 1000) FT-IR

Table 1 XRD data of ZrO_2 nanoparticles

No.	2θ	d value	FWHM (deg)	Phase data	h	k	l
1	30.22	2.95	1.71	Arkelite	1	1	1
2	35.03	2.56	1.71	Arkelite	2	0	0
3	50.39	1.81	1.71	Arkelite	2	2	0
4	59.89	1.54	1.71	Arkelite	3	1	1
5	62.84	1.48	1.71	Arkelite	2	2	2
6	74.02	1.28	1.71	Arkelite	4	0	0
7	81.99	1.17	1.71	Arkelite	3	3	1
8	84.60	1.14	1.71	Arkelite	4	2	0
9	31.17	2.87	1.67	Zr	1	0	0
10	35.08	2.56	1.67	Zr	0	0	2
11	35.89	2.50	1.67	Zr	1	0	1
12	47.62	1.91	1.67	Zr	1	0	2
13	55.47	1.66	1.67	Zr	1	1	0
14	63.45	1.46	1.67	Zr	1	0	3
15	65.01	1.43	1.67	Zr	2	0	0
16	67.35	1.39	1.67	Zr	1	1	2
17	67.85	1.38	1.67	Zr	2	0	1
18	74.13	1.27	1.67	Zr	0	0	4
19	76.07	1.25	1.67	Zr	2	0	2
20	82.58	1.16	1.67	Zr	1	0	4
21	89.21	1.09	1.67	Zr	2	0	3

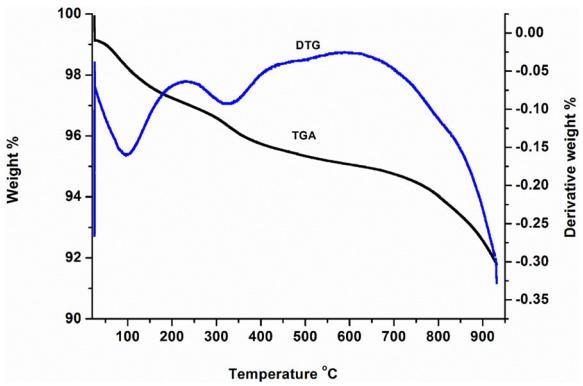

Fig. 4 Comparison of the TGA/DTG curves of the ZrO_2 nanoparticles

instrument over a range of 4000–400 cm^{-1} and a resolution of 4 cm^{-1}.

Electrochemical studies

Electrochemical measurements were observed under three electrodes. While silver–silver chloride (Ag/AgCl) electrode was used as the reference electrode, zirconia nanoparticles coated on glassy carbon were used as a working electrode and Pt wire was used as a counter electrode. 0.03 g of ZrO_2 was ultra-sonicated in 0.5 ml 1 wt% Nafion in absolute ethanol for 30 min, pipetted a 0.05-ml suspension onto the glassy carbon electrode and dried at ambient temperature (Dong et al., 2009). The cyclic voltammograms (CVs) and electrochemical impedance spectroscopy (EIS) were observed under 2 M of potassium chloride (KCl) and sodium nitrate ($NaNO_3$)

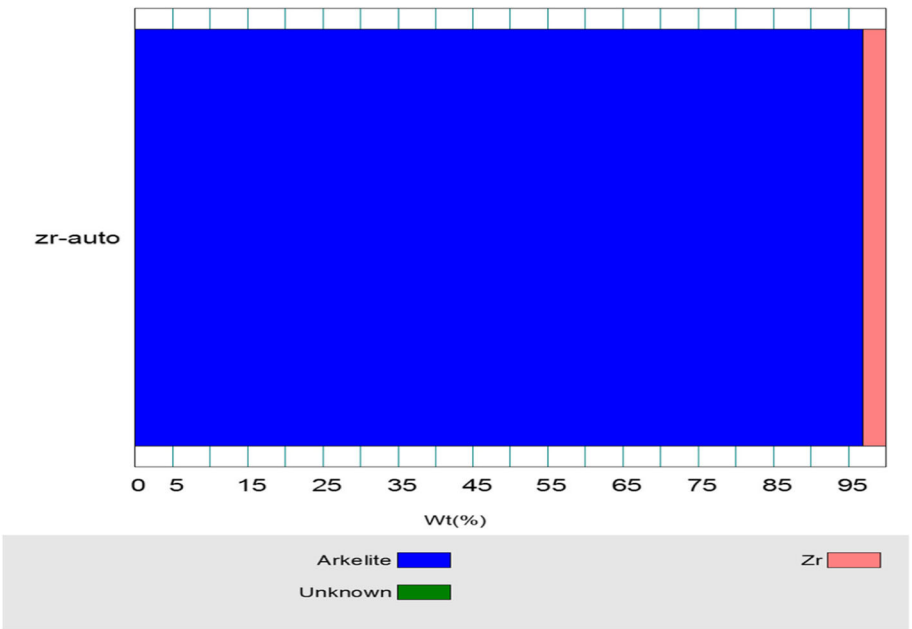

Fig. 3 Composition of zirconia and Arkelite nanostructure

electrolytes. The scan rates used were 10 mV s^{-1}, 20 mV s^{-1}, 30 mV s^{-1}, 50 mV s^{-1} and 100 mV s^{-1} with the CVs test ranges from − 0.15 to 0.55 V vs. EIS measurements obtained under the frequency range of 100 kHz to 0.01 Hz.

Results and discussion

Crystallographic analysis of ZrO_2

The XRD pattern of ZrO_2 nanoparticles synthesised by means of the hydrothermal method is shown in Fig. 1. The XRD results of zirconia nanoparticles show a pure cubic phase with the first space group (*Fm*-3*m*, $Z = 4$, DB card no. 5000038) and the second space group (*Im*-3*m*, $Z = 1$, DB card no. 9008559), in Fig. 2 (Chen et al., 2005). The broadening XRD peak shows that the crystallite size of ZrO_2 was fine nanoparticles and more crystallised. This may be due to the effect of the temperature on the crystallinity of the nanoparticles. The ZrO_2 nanoparticles show that the diffraction characteristic peaks at 2θ are 30.2°, 35.0°, 50.4°, 59.9°, 62.8°, 74.0°, 82.0° and 84.6°, which correspond with the planes (1 1 1), (2 0 0), (2 2 0), (3 1 1), (2 2 2), (4 0 0), (3 3 1) and (4 2 0) (Davar, Hassankhani, & Loghman-Estarki, 2013; Tahmasebpour, Babaluo, & Aghjeh, 2008), with diffraction peaks in the spectra indexed as cubic with lattice constants $a = 5.1144$, $b = 5.1144$, $c = 5.1144$ and $\beta = 90.0^{o}$ as indicated in Table 1 and Fig. 1. Table 1 indicates the diffraction characteristic peaks of 31.2°, 35.0°, 47.6°, 55.5°, 63.5°, 65.0°, 67.3°, 67.9°, 75.1°, 76.1°, 82.6° and 89.2° at 2θ, which correspond with the planes (1 0 0), (0 0 2), (1 0 1), (1 0 2), (1 1 0), (1 0 3), (2 0 0), (1 1 2), (2 0 1), (0 0 4), (2 0 2), (1 0 4) and (2 0 3), with diffraction peaks in the spectra indexed as cubic with lattice constants $a = 3.6153$, $b = 3.6153$, $c = 3.615$ and $\beta = 90.0^{o}$. These high-temperature phases (cubic and tetragonal) are unstable at ambient temperature, but some researchers have found that if the particle size is less than 30 nm, the tetragonal phase can stabilise at room temperature (Nishizawa, Yamasaki, Matsuoka, & Mitsushio, 1982). Nishizawa et al. (1982) found that using the hydrothermal method at 130 °C can transform amorphous ZrO_2 into crystalline form, but in this study, we found that cubic crystallites form under the lower temperature of 120 °C. Noh, Seo, Kim, and Lee (2003) produced ZrO_2 nanocrystals with anisotropic shapes and various crystal structures when using the hydrothermal process (Noh et al., 2003).

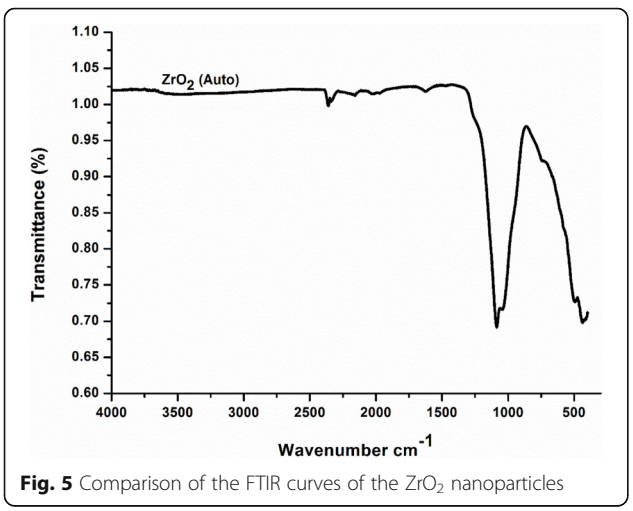

Fig. 5 Comparison of the FTIR curves of the ZrO_2 nanoparticles

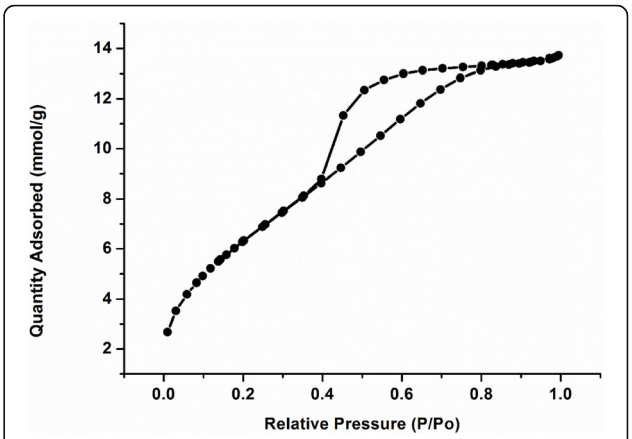

Fig. 6 N_2 adsorption/desorption isotherms of ZrO_2 nanoparticles

The cubic zirconia consisted of 8 Zr atoms and 12 O atoms to form cubic ball-like structures, whereas the monoclinic zirconia had 8 Zr atoms and 11 O atoms in its nanostructure (Christensen & Carter, 1998; Nagarajan, Saravanakannan, & Chandiramouli, 2014). In Fig. 2a, b, the illustration shows the crystalline unit cells of the β(Zr) phases of zirconia that are in a stable phase, with a space group of (*Im*3-*m*) (Maimaitiyili et al., 2014), and δ(뀙뀾뀿 1.66) phases of zirconia that are in a stable phase, with a space group of (*Fm*3-*m*) (Maimaitiyili et al., 2014). The β-Zr phase lattice parameters are ($a = b = c = 3.6153$ Å) at 120 °C. This is bigger than ($a = b = c = 3.6090$ Å) at 863 °C, which was obtained by Zuzek, Abriata, San-Martin, and Manchester (1990), as seen in Fig. 2a. Figure 2b shows the δ(뀙뀾뀿1.66) phases lattice parameters are ($a = b = c = 5.1144$ Å) at 120 °C, which is bigger than ($a = b = c = 4.8051$ Å) at 500 °C (Singh, Ståhle, Massih, & Shmakov, 2007). The results show that we obtained the expanded structure at the lower temperature of 120 °C, using the hydrothermal method. The difference between the cubic with symmetry (*Fm*3-*m*) and (*Im*3-*m*) is the alternating distortion of the O atom columns along the 14 axes, as indicated in Fig. 2a, b, as it can be orientated as a face-centred cubic (FCC) or body-centred cubic (BCC). By using the hydrothermal method, it is possible to stabilise the multi-cubic phase at a

Table 2 BET surface area for ZrO_2

Samples	BET surface area (m^2/g)	Pore size (nm)	Pore volume (cm^3/g)
$ZrO_{2(auto)}$	543	3.5	0.5

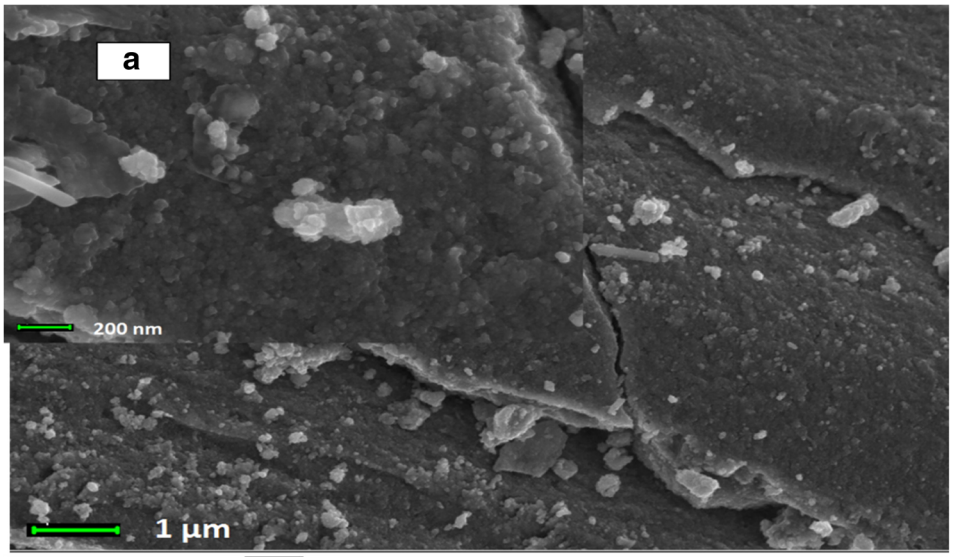

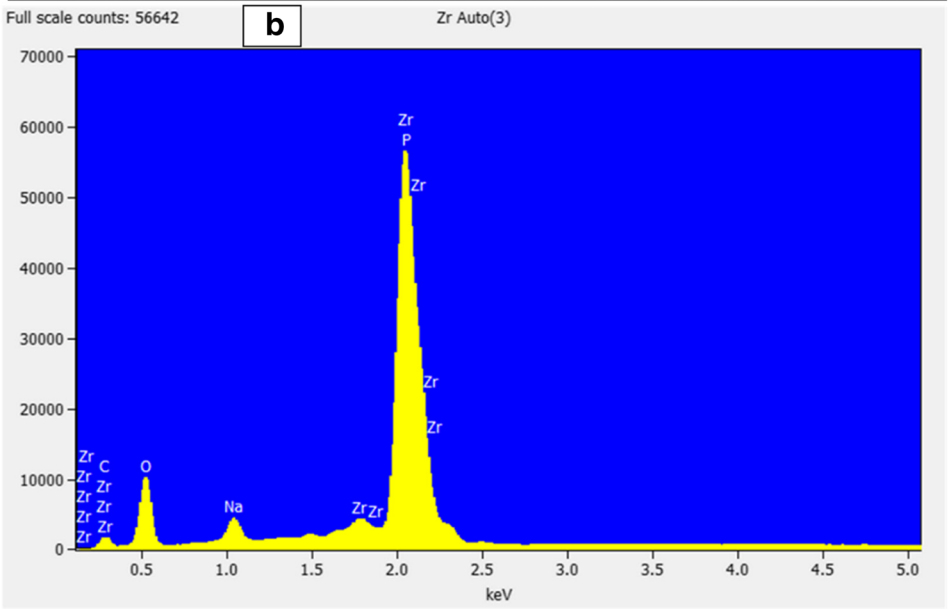

c

Element Line	Weight %	Weight % Error	Atom %	Atom % Error
C K	11.33	± 0.20	25.39	± 0.44
O K	32.02	± 0.18	53.85	± 0.30
Na K	3.59	± 0.05	4.20	± 0.06
P K	1.57	± 0.29	1.36	± 0.25
Zr L	51.49	± 0.40	15.19	± 0.12
Total	100.00		100.00	

Fig. 7 **a** Scanning electron microscopy, **b** EDAX and **c** Elements of ZrO_2

lower temperature of 120 °C. The compositions of Zr and Arkelite are presented in Fig. 3.

Powder thermo-gravimetric analysis and derivative thermo-gravimetric

The TGA and derivative thermo-gravimetric (DTG) curves of the decomposition of zirconia nanoparticles are seen in Fig. 4. Figure 4 shows that the weight loss on TGA curves undergoes three stages. The initial stages of weight loss, at 100 °C, are due to the desorption of physically adsorbed water. The second stage of decomposition, from 100 to 650 °C, corresponds with the removal of decomposing terminal hydroxyl groups bonded to the surface of the zirconia (Gil, Mas, Lerma, & Vercher, 2015). The third stage of decomposition occurred between 650 and 920 °C, which corresponds with the degradation of the material. Zirconia nanoparticles stop losing weight at 920 °C, with a total mass of 7.5%. These results confirm the thermal stability of zirconia nanoparticles synthesised by using the hydrothermal method, as it shows little degradation. This is very important in the modification of Nafion membrane for fuel cell application, as it will enhance the thermal stability of the membrane (Wang, Tan, Li, Sun, & Zhang, 2006). The thermal decomposition of the DTG process occurs during two weight loss stages, as seen in Fig. 4. The DTG curve in Fig. 4 reveals the first weight loss at 80 °C, due to the evaporation of hydrated water with a mass loss of 2%. The second stage of thermal decomposition, at 340 °C, with a mass loss of 1%, was due to sulfate and carbonaceous phase decomposition.

FT-IR spectrum of ZrO_2 nanoparticles

The FT-IR spectrum of the zirconia nanoparticle samples in the range 400–4000 cm^{-1} was observed (Fig. 5) in order to ascertain its molecular nature. The FT-IR spectrum of the ZrO_2 nanoparticles in Fig. 5 shows a strong absorption with a maximum peak at 475 cm^{-1}, due to the Zr–O vibration, which confirms the formation of the ZrO_2 structure (Chen, Yin, Wang, Liu, & Wang, 2005; Escribano et al., 2003; Gengelbach & Spears, 1998). The absorption peak in the region of 1380 cm^{-1} corresponds with O–H bonding, while a peak in the region of 1553 cm^{-1} may be due to the adsorbed moisture. A peak in the region of 3500 cm^{-1} is attributed to the stretching of O–H groups, characteristic of a highly hydrated compound (Guo, Chen, & Ying, 2004). This highly hydrated compound enhances water uptake within the modified membranes with zirconia, which gives potential applications in fuel cells. The peak observed at 2350 cm^{-1} and 2320 cm^{-1} corresponds with the structural O–H stretching of the nanomaterials. The peak observed in the region of 1550 cm^{-1} is due to the adsorbed moisture (Piszczek, Radtke, Grodzicki, Wojtczak, & Chojnacki, 2007; Yashima et al., 1997). Symmetric frequencies of Zr–OH were observed at 1080 cm^{-1} (Tai, Hsiao, & Chiu, 2004).

Brunauer–Emmett–Teller

Figure 6 and Table 2 show the BET surface area of the zirconia nanoparticles prepared by the hydrothermal method at 120 °C. The obtained BET surface area was 543 m^2/g, which is larger than the reported values (Ahniyaz, Fujiwara, Fujino, & Yoshimura, 2004; Tahir et al., 2007), and pore volume of 0.5 cm^3/g, as seen in Table 2. The N_2 adsorption/desorption isotherms of mesoporous zirconia nanoparticles appear in Fig. 6. This isotherm can be classified as type IV, which indicates the mesoporous nature of the materials (Gregg & Sing, 1982), with type A indicating the hysteresis loops (Everett & Stone, 1958). Figure 6 shows that the isotherms of zirconia nanoparticles start at a relative pressure of 0.4 and extend to a relative pressure close to 1. The hydrothermal method produces mesoporous zirconia material with a higher specific surface area, indicating thermal stability, as confirmed by the TGA/DTG, and producing the more cubic stabilised crystal structure. These high surface area and high porosity zirconia nanoparticles are important parameters in the preparation of modified Nafion nanocomposite membrane to be applied in fuel cells.

Elemental and morphological analysis

Figure 7 shows SEM images of ZrO_2 nanoparticles, which were taken at a high magnification scale bar of 200 nm and 1 μm. It can be seen in Fig. 7a that many ZrO_2 nanoparticles were aggregated in the form of spherical and nanorod shapes. Nevertheless, most of the nanoparticles are aggregated in the form of nanospheres. This agglomeration occurred due to the formation of unstable and ultra-fine nuclei that have a strong tendency to be stable when agglomerated. The elemental composition of ZrO_2 nanoparticles has been confirmed by EDAX spectra, as shown in Fig. 7b, c. Figure 7c shows the highest value of zirconia (Zr (51.5%)) and oxygen (O (32.0%)) elements that represent the presence of zirconia and oxygen in the synthesised sample. Figure 7c shows 11.3% carbon (C), which indicates the high usage of carbon tape as a supporting material for SEM-EDX analysis. Furthermore, small traces of sodium (Na (3.6%)) were also found, as seen in Fig. 7b, c, due to the use of sodium hydroxide in the preparation of the zirconia nanoparticles.

Cyclic voltammetry behaviour of zirconia nanoparticles

Figure 8 shows the electrochemical behaviour of ZrO_2 nanoparticles, under the cyclic voltammetry and EIS using the $NaNO_3$ and KCl electrolytes. Figure 8a shows the cyclic voltammetry behaviours of ZrO_2 in $NaNO_3$

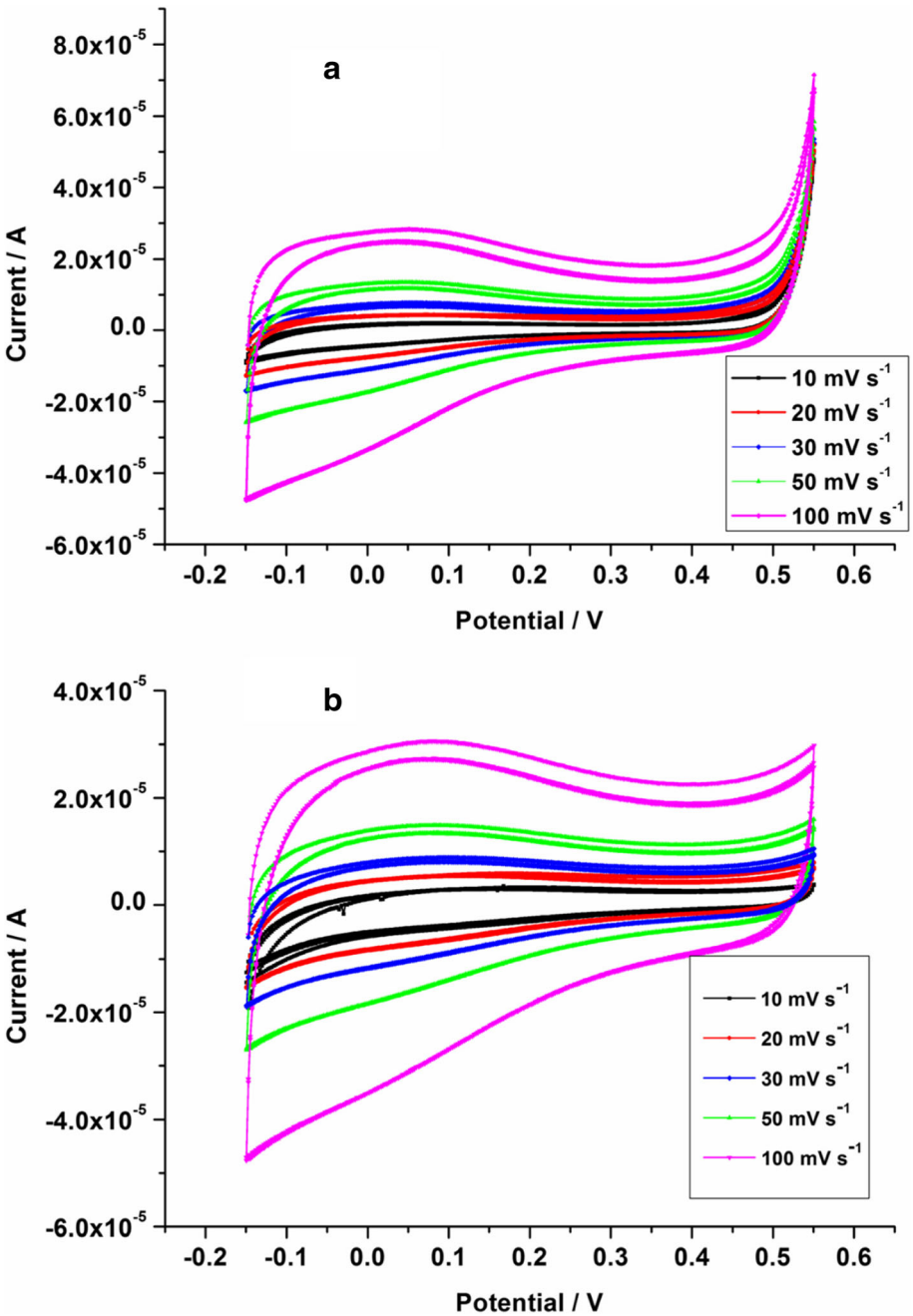

Fig. 8 Cyclic voltammetry's of ZrO_2 at a scanning rate of 10 mV s^{-1}, 20 mV s^{-1}, 30 mV s^{-1}, 50 mV s^{-1} and 100 mV s^{-1} in **a** $NaNO_3$ and **b** KCl

electrodes at the scan rates of 10 mV s^{-1}, 20 mV s^{-1}, 30 mV s^{-1}, 50 mV s^{-1} and 100 mV s^{-1}. Figure 8a, b shows that CVs of ZrO_2 obtained a rectangular shape, revealing the ideal capacitive behaviour (Tran & Kalra, 2013), with the increased redox peak current; this may due to the transfer of electrons. Figure 8a indicates that when the scan rate increases, the current also increases, expected for a pure capacitor due to the resistance effects down the pores (Nasibi, Golozar, & Rashed, 2012). Figure 8b shows the near-rectangular cyclic voltammetry curves at low and high scan rates. The CV shape at a low scan rate is distorted, which may be due to the high surface area of ZrO_2 nanoparticles that enhanced the electronic conductivity and reversible redox reactions at the electrode surface (Yu et al., 2011). It can be concluded that ZrO_2 nanoparticles composited in Nafion membrane can be considered a promising electrolyte in the application of fuel cell. Both KCl and $NaNO_3$ obtain a high ionic radius

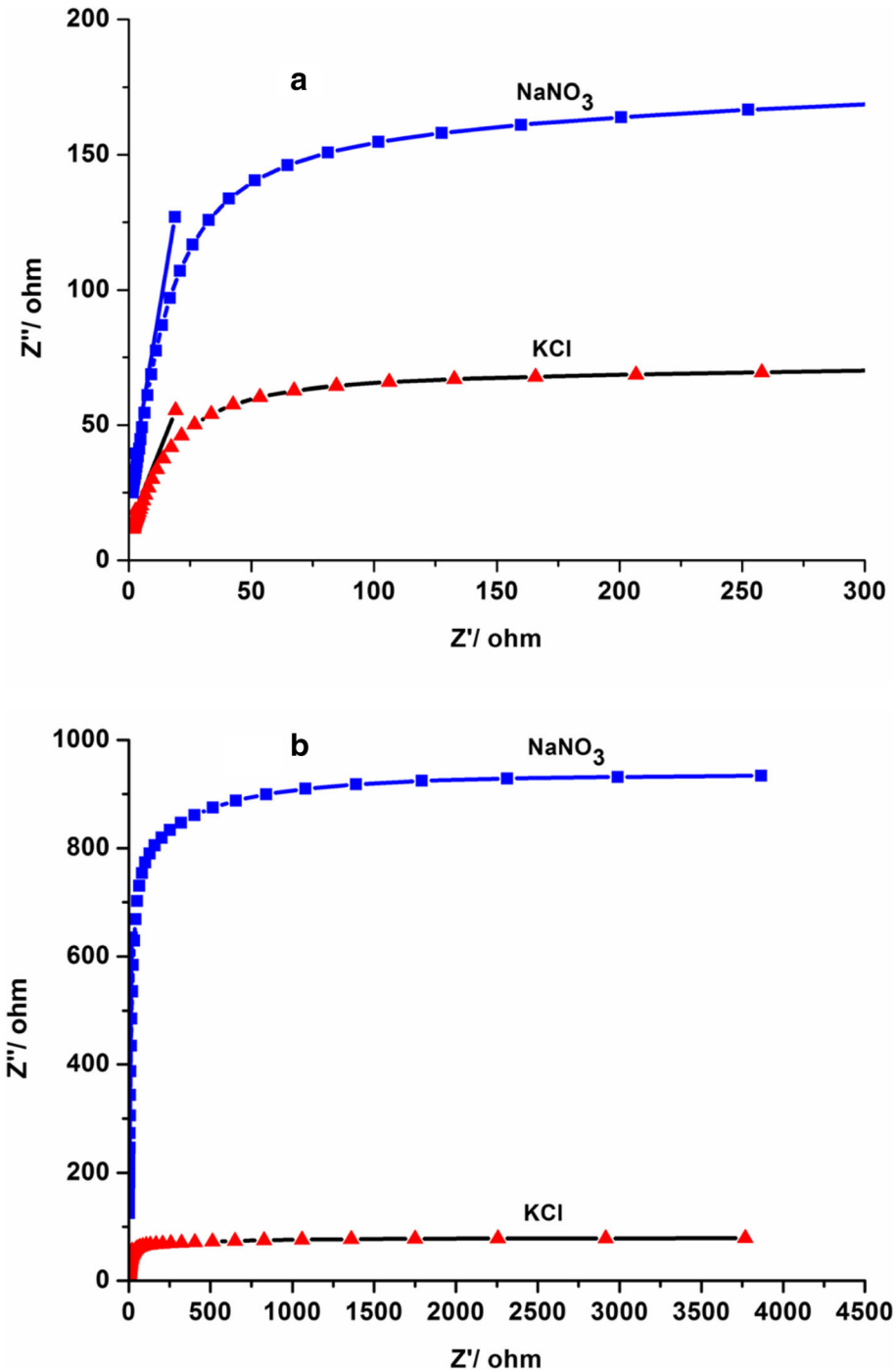

Fig. 9 Nyquist plots of ZrO_2 in $NaNO_3$ and KCl electrolytes at a high (**a**) and low (**b**) frequency

of anions which is a very important parameter for capacitance behaviour. As seen in Fig. 8b, when increasing the scan rate to 100 mV s^{-1}, the current versus potential relation of CV would deviate from the classical square waveform expected for a pure capacitor (Conway & Pell, 2002). Figure 8b shows that at the scan rate of 10 mV s^{-1}, the rectangular curve is too small and distorted. When the scan rate increased to 100 mV s^{-1}, the CV curves still retain a nearly rectangular shape without obvious distortion. Furthermore, the CVs of KCl and $NaNO_3$ electrolytes show that the capacitance increases in higher surface area and smallest particle size. Figure 9 illustrates the Nyquist plot of the ZrO_2 in 2 M $NaNO_3$ and 2 M KCl electrolytes at high frequency and low

frequency. Figure 9a, b indicates that the curve of ZrO_2 in 2 M $NaNO_3$ is higher when compared to 2 M KCl, which may be due to its higher electrical conductivity. As the diameter decreases, the conductivity increases (Mokhtaruddin, Mohamad, Loh, & Kadhum, 2016). The Nyquist plots in Fig. 9a, b have nearly vertical lines in the low-frequency region, indicating an almost ideal capacitor response. The lower Nyquist plots at lower and higher frequency of 2 M KCl show the increases of the electron transfer. The curves have a linear region at low frequencies, indicative of capacitor behaviour as seen in Fig. 9b. The electrolyte diffusion resistances of different zirconia are slightly different, but the charge transfer resistance of zirconia nanoparticles is smaller than the conventional zirconia, according to the size of the radius in Fig. 9b.

Conclusion

The hydrothermal method was found to be the suitable method to synthesise a high surface area zirconia, as confirmed by BET results which reveal a high specific surface area of 543 m^2/g and pore volume of 0.5 cm^3/g. The XRD results indicate the pure cubic nanocrystalline phase of zirconia, with the different structure orientations of FCC and BCC in one sample. High-resolution SEM images of ZrO_2 nanoparticles confirm the presence of nanospheres and nanobars. Moreover, the EDAX spectra show the highest value of zirconia (Zr (51.5%)) and oxygen (O (32.0%)) elements that represent the presence of zirconia and oxygen in the synthesised sample. Furthermore, the TGA/DTG results show the improvements in thermal stability with little degradation. This is very important in the modification of Nafion membrane for fuel cell application, as it will enhance the thermal stability of the membrane. The zirconia nanoparticles maintain a rectangular shape with good cycling and reversibility stability at the scan rate of 100 $mV\,s^{-1}$. The CV rectangular shape reveals the ideal capacitive behaviour, with the increased redox peak current, due to the transfer of electrons. The Nyquist plots of 2 M $NaNO_3$ and KCl electrolytes have higher electric conductivity at lower and higher frequency. However, the Nyquist plots of 2 M $NaNO_3$ are higher than those of 2 M KCl electrolytes, which may be due to its higher electrical conductivity. It can be concluded that ZrO_2 nanoparticles composited in Nafion membrane can be considered a promising electrolyte in the application of fuel cell.

Abbreviations

0D: Zero-dimensional; 1D: One-dimensional; 3D: Three-dimensional; AAO: Anodic aluminium oxide; BCC: Body-centred cubic; BET: Brunauer–Emmett–Teller; C: Cubic; CV: Cyclic voltammetry; EIS: Electrochemical impedance spectroscopy; FCC: Face-centred cubic; FTIR: Fourier transform infrared; KCl: Potassium chloride; M: Monoclinic; $NaNO_3$: Sodium nitrate; NaOH: Sodium hydroxide; SEM: Scanning electron microscopy; T: Tetragonal; TGA: Thermal gravimetric analysis; XRD: X-ray diffraction; ZrO_2: Zirconium oxide; $ZrOCl_2{\cdot}8H_2O$: Zirconium oxychloride hydrate

Acknowledgements

The authors would like to acknowledge and thank the National Research Foundation of South Africa (NRF) and the University of South Africa (AQIP) for their financial support.

Funding

National Research Funding (Grant UID: 95333) and University of South Africa (Academic Qualification Improvement Programme (AQIP))

Availability of data and materials

All data analysed during this study are available from the corresponding author on request.

Authors' contributions

The authors read, corrected and approved the final manuscript.

Competing interests

The authors declare that they have no competing interests.

Publisher's Note

Author details

[1]Department of Chemical Engineering, University of South Africa, Private Bag X6, Florida 1710, South Africa. [2]Department of Physics, University of South Africa, Private Bag X6, Florida 1710, South Africa. [3]Department of Mechanical and Industrial Engineering, University of South Africa, Private Bag X6, Florida 1710, South Africa.

Received: 20 February 2019 Accepted: 30 April 2019
Published online: 22 May 2019

References

Ahniyaz, A., Fujiwara, T., Fujino, T., & Yoshimura, M. (2004). Low-temperature direct synthesis of CeO2–ZrO2 solid solution nanoparticles by a hydrothermal method. *Journal of Nanoscience and Nanotechnology, 4*, 233–238.

Arantes, T. M., Mambrini, G. P., Stroppa, D. G., Leite, E. R., Longo, E., Ramirez, A. J., & Camargo, E. R. (2010). Stable colloidal suspensions of nanostructured zirconium oxide synthesized by hydrothermal process. *Journal of Nanoparticle Research, 12*, 3105–3110.

Babu, C. R., Reddy, N. R. M., & Reddy, K. (2015). Synthesis and characterization of high dielectric nano zirconium oxide. *Ceramics International, 41*, 10675–10679.

Behbahani, A., Rowshanzamir, S., & Esmaeilifar, A. (2012). Hydrothermal synthesis of zirconia nanoparticles from commercial zirconia. *Procedia Engineering, 42*, 908–917.

Cao, H., Qiu, X., Luo, B., Liang, Y., Zhang, Y., Tan, R., Zhao, M., & Zhu, Q. (2004). Synthesis and room-temperature ultraviolet photoluminescence properties of zirconia nanowires. *Advanced Functional Materials, 14*, 243–246.

Chen, H., Gu, J., Shi, J., Liu, Z., Gao, J., Ruan, M., & Yan, D. (2005). A composite surfactant route for the synthesis of thermally stable and hierarchically porous zirconia with a nanocrystallized framework. *Advanced Materials, 17*, 2010–2014.

Chen, S., Yin, Y., Wang, D., Liu, Y., & Wang, X. (2005). Structures, growth modes and spectroscopic properties of small zirconia clusters. *Journal of Crystal Growth, 282*, 498–505.

Christensen, A., & Carter, E. A. (1998). First-principles study of the surfaces of zirconia. *Physical Review B, 58*, 8050.

Conway, B., & Pell, W. (2002). Power limitations of supercapacitor operation associated with resistance and capacitance distribution in porous electrode devices. *Journal of Power Sources, 105*, 169–181.

Davar, F., Hassankhani, A., & Loghman-Estarki, M. R. (2013). Controllable synthesis of metastable tetragonal zirconia nanocrystals using citric acid assisted sol–gel method. *Ceramics International, 39*, 2933–2941.

Dercz, G., Prusik, K., & Pajak, L. (2008). X-ray and SEM studies on zirconia powders. *JAMME, 31*, 408–414.

Dong, W.-S., Lin, F.-Q., Liu, C.-L., & Li, M.-Y. (2009). Synthesis of ZrO2 nanowires by ionic-liquid route. *Journal of Colloid and Interface Science, 333*, 734–740.

Dwivedi, R., Maurya, A., Verma, A., Prasad, R., & Bartwal, K. (2011). Microwave assisted sol–gel synthesis of tetragonal zirconia nanoparticles. *Journal of Alloys and Compounds, 509*, 6848–6851.

Escribano, V. S., López, E. F., Panizza, M., Resini, C., Amores, J. M. G., & Busca, G. (2003). Characterization of cubic ceria–zirconia powders by X-ray diffraction and vibrational and electronic spectroscopy. *Solid State Sciences, 5*, 1369–1376.

Everett, D. H., & Stone, F. S. (1958). The structure and properties of porous materials (Proceedings of the tenth symposium of the Colston Research Society held in University of Bristol). Butterworths, 10.

Ge, J., Ye, Y. D., Yao, H. B., Zhu, X., Wang, X., Wu, L., Wang, J. L., Ding, H., Yong, N., & He, L. H. (2014). Pumping through porous hydrophobic/oleophilic materials: An alternative technology for oil spill remediation. *Angewandte Chemie, 126*, 3686–3690.

Gengelbach, G., & Spears, J. (1998). Effects of dietary copper and molybdenum on copper status, cytokine production, and humoral immune response of calves 1. *Journal of Dairy Science, 81*, 3286–3292.

Gil, E., Mas, Á., Lerma, C., & Vercher, J. (2015). Exposure factors influence stone deterioration by crystallization of soluble salts. *Advances in Materials Science and Engineering, 2015*, 1–10.

Gregg, S., & Sing, K. (1982). *W. Adsorption surface area and porosity, 2nd.* London: Academic.

Guo, G.-Y., Chen, Y.-L., & Ying, W.-J. (2004). Thermal, spectroscopic and X-ray diffractional analyses of zirconium hydroxides precipitated at low pH values. *Materials Chemistry and Physics, 84*, 308–314.

Hamling, D. (1997). *Using ceramic-fiber materials in corrosive environments*. *American Ceramic Society Bulletin, 76*, 79–82.

Ibáñez, R. L., Martin, F., Ramos-Barrado, J., & Leinen, D. (2006). Optimization of spray pyrolysis zirconia coatings on aluminized steel. *Surface and Coatings Technology, 200*, 6368–6372.

Kalkur, T., & Lu, Y. (1992). Electrical characteristics of ZrO 2-based metal-insulator-semiconductor structures on p-Si. *Thin Solid Films, 207*, 193–196.

Kumari, L., Du, G., Li, W., Vennila, R. S., Saxena, S., & Wang, D. (2009). Synthesis, microstructure and optical characterization of zirconium oxide nanostructures. *Ceramics International, 35*, 2401–2408.

Lumpkin, G. R. (1999). Physical and chemical characteristics of baddeleyite (monoclinic zirconia) in natural environments: An overview and case study. *Journal of Nuclear Materials, 274*, 206–217.

Maimaitiyili, T., Steuwer, A., Blomquist, J., Matthew, B., Olivier, Z., Andrieux, J., Bjerkén, C., & Fabienne, R. (2014). In-situ hydrogen charging of zirconium powder to study isothermal percipitation of hydrides and determination of Zr-hydride crystal structure. *arXiv preprint arXiv, 1408*, 4665.

Mokhtaruddin, S. R., Mohamad, A. B., Loh, K. S., & Kadhum, A. A. H. (2016). Thermal properties and conductivity of Nafion-zirconia composite membrane. *Malaysian Journal of Analytical Sciences, 20*, 670–677.

Monaco, C., Tucci, A., Esposito, L., & Scotti, R. (2013). Microstructural changes produced by abrading Y-TZP in presintered and sintered conditions. *Journal of Dentistry, 41*, 121–126.

Nagarajan, V., Saravanakannan, V., & Chandiramouli, R. (2014). Quantum chemical insights on structural and electronic properties of anionic, cationic and neutral ZrO2 nanostructures. *International Journal of ChemTech Research, 6*, 2962–2970.

Nasibi, M., Golozar, M. A., & Rashed, G. (2012). Nano zirconium oxide/carbon black as a new electrode material for electrochemical double layer capacitors. *Journal of Power Sources, 206*, 108–110.

Nishizawa, H., Yamasaki, N., Matsuoka, K., & Mitsushio, H. (1982). Crystallization and transformation of zirconia under hydrothermal conditions. *Journal of the American Ceramic Society, 65*, 343–346.

Noh, H.-J., Seo, D.-S., Kim, H., & Lee, J.-K. (2003). Synthesis and crystallization of anisotropic shaped ZrO 2 nanocrystalline powders by hydrothermal process. *Materials Letters, 57*, 2425–2431.

Piszczek, P., Radtke, A., Grodzicki, A., Wojtczak, A., & Chojnacki, J. (2007). The new type of [Zr 6 (μ 3-O) 4 (μ 3-OH) 4] cluster core: Crystal structure and spectral characterization of [Zr 6 O 4 (OH) 4 (OOCR) 12](R= Bu t, C (CH 3) 2 et). *Polyhedron, 26*, 679–685.

Reddy, B. M., & Khan, A. (2005). Recent advances on TiO2-ZrO2 mixed oxides as catalysts and catalyst supports. *Catalysis Reviews, 47*, 257–296.

Sigwadi, R., Dhlamini, S., Mokrani, T., & Nonjola, P. (2017). Effect of synthesis temperature on particles size and morphology of zirconium oxide nanoparticle. *Journal of Nano Research, 50*, 18–31.

Singh, A. K., & Nakate, U. T. (2014). Microwave synthesis, characterization, and photoluminescence properties of nanocrystalline zirconia. *The Scientific World Journal, 2014*, 1–7.

Singh, R. N., Ståhle, P., Massih, A. R., & Shmakov, A. (2007). Temperature dependence of misfit strains of δ-hydrides of zirconium. *Journal of Alloys and Compounds, 436*, 150–154.

Tahir, M. N., Gorgishvili, L., Li, J., Gorelik, T., Kolb, U., Nasdala, L., & Tremel, W. (2007). Facile synthesis and characterization of monocrystalline cubic ZrO2 nanoparticles. *Solid State Sciences, 9*, 1105–1109.

Tahmasebpour, M., Babaluo, A., & Aghjeh, M. R. (2008). Synthesis of zirconia nanopowders from various zirconium salts via polyacrylamide gel method. *Journal of the European Ceramic Society, 28*, 773–778.

Tai, C. Y., Hsiao, B.-Y., & Chiu, H.-Y. (2004). Preparation of spherical hydrous-zirconia nanoparticles by low temperature hydrolysis in a reverse microemulsion. *Colloids and Surfaces A: Physicochemical and Engineering Aspects, 237*, 105–111.

Tran, C., & Kalra, V. (2013). Fabrication of porous carbon nanofibers with adjustable pore sizes as electrodes for supercapacitors. *Journal of Power Sources, 235*, 289–296.

Wang, L., Cai, K., Wang, Y., Yin, J., Li, H., & Zhou, C. (2009). Preparation and characterization of tetragonal-ZrO 2 nanopowders by a molten hydroxides method. *Ceramics International, 35*, 2499–2501.

Wang, S., Tan, Z., Li, Y., Sun, L., & Zhang, T. (2006). Synthesis, characterization and thermal analysis of polyaniline/ZrO 2 composites. *Thermochimica Acta, 441*, 191–194.

William, D., Callister, JR., David, G.R. (2012). Fundamentals of materials science and engineering: An integrated approach. Hoboken: Wiley.

Xu, H., Qin, D.-H., Yang, Z., & Li, H.-L. (2003). Fabrication and characterization of highly ordered zirconia nanowire arrays by sol–gel template method. *Materials Chemistry and Physics, 80*, 524–528.

Yashima, M., Kato, T.-A., Kakihana, M., Gulgun, M. A., Matsuo, Y., & Yoshimura, M. (1997). Crystallization of hafnia and zirconia during the pyrolysis of acetate gels. *Journal of Materials Research, 12*, 2575–2583.

Yu, G., Hu, L., Liu, N., Wang, H., Vosgueritchian, M., Yang, Y., Cui, Y., & BAO, Z. (2011). Enhancing the supercapacitor performance of graphene/MnO2 nanostructured electrodes by conductive wrapping. *Nano Letters, 11*, 4438–4442.

Zhu, Y.-F., Shi, L., Liang, J., Hui, D., & Lau, K.-T. (2008). Synthesis of zirconia nanoparticles on carbon nanotubes and their potential for enhancing the fracture toughness of alumina ceramics. *Composites Part B: Engineering, 39*, 1136–1141.

Zuzek, E., Abriata, J., San-Martin, A., & Manchester, F. (1990). The H-Zr (hydrogen-zirconium) system. *Journal of Phase Equilibria, 11*, 385–395.